https://doi.org/10.5194/egusphere-2026-2713
Preprint. Discussion started: 1 June 2026

Local dissipation efficiency of internal tides at key topographic features in the South China Sea

Zuqing Yuan[1]⋆, Hui Sun[1]⋆, Qingxuan Yang[1,2], Fenyuan Han[1], Jianing Li[1]

[1]State Key Laboratory of Physical Oceanography, Ocean University of China, Qingdao, China.
[2]Laboratory for Ocean Dynamics and Clinate, Qingdao Marine Science and Technology Center, Qingdao, China.
⋆These authors contributed equally to this work.

Correspondence to: Qingxuan Yang (yangqx@ouc.edu.cn)

Abstract. The local dissipation efficiency of internal tides, q, is a critical parameter in tidal mixing parameterizations. However, the conventionally adopted constant value ($q \approx 0.3$) in large-scale ocean models neglects its significant spatiotemporal variability. Based on the MITgcm LLC4320 simulation, the internal tidal energy budgets at the Luzon Strait (a source region, LS) and the Nansha Islands (a sink region, Nansha) in the South China Sea (SCS) are analyzed. Results indicate that the barotropic-to-baroclinic energy conversion in the LS reaches approximately 45 GW, with semidiurnal constituents accounting for roughly 60%, due to the resonance over the double-ridge topography. The value of q in the LS fluctuates between 0.3 and 0.7, primarily modulated by the high-mode local dissipation. Local internal tide generation around the Nansha Islands is less than 1.5 GW; however, this region experiences significant convergence of internal tidal energy flux, which elevates the value of q to generally greater than 1 and occasionally exceeding 2.5. Modal analysis confirms that the intensified dissipation over the Nansha Islands originates predominantly from topographic scattering and breaking of mode-1 internal tides from the far field. Parameterizations for q are developed based on both physical factors and data-driven algorithms, both of which successfully capture the macroscopic clustering of q. In the LS, q is modulated by near-field factors such as the barotropic tidal forcing and the local dissipation of high-mode internal tides. Conversely, q around the Nansha Islands is primarily contributed by mode-1 internal tidal energy coming from the far field, highlighting the jointly modulation of local extreme dissipation by far-field beam interference and nonlinear topographic scattering.

1 Introduction

Diapycnal mixing in the ocean is a key dynamical process that maintains the global ocean stratification, shapes the meridional overturning circulation, and regulates the transport of heat, energy, and nutrients (Munk and Wunsch, 1998; Wunsch and Ferrari, 2004). In the deep ocean, the interaction of barotropic tides with rough topography generates internal tides, which are widely regarded as the primary mechanical energy source furnishing deep-ocean mixing (Egbert and Ray, 2000; Garrett and Kunze, 2007; Ferrari and Wunsch, 2009). It is estimated that approximately 1 TW of barotropic tidal

https://doi.org/10.5194/egusphere-2026-2713
Preprint. Discussion started: 1 June 2026

energy is converted into internal tides, accounting for roughly half of the total energy required to maintain global abyssal mixing (Egbert and Ray, 2003; Nycander, 2005). However, the generated internal tides generally break via nonlinear interactions, cascading energy down to the turbulence scale, which is ultimately dissipated to drive diapycnal mixing (Waterhouse et al., 2014). A fraction of the generated internal tidal energy dissipates near the generation sites through high-mode breaking, while the remainder radiates into the far field as low-mode internal tides and eventually dissipates due to wave-wave interactions and topographic scattering (St. Laurent and Garrett, 2002; MacKinnon et al., 2017). Therefore, accurately quantifying the spatiotemporal distribution of the local internal tidal dissipation is crucial for improving the performance of ocean circulation and climate models (Melet et al., 2016; de Lavergne et al., 2020).

In state-of-the-art climate-scale ocean models, the mixing induced by internal tidal breaking cannot be explicitly resolved due to limitations in grid resolution and must therefore be parameterized (Jayne, 2009). The local dissipation efficiency, q, is a decisive dimensionless parameter defined as the ratio of the internal tidal energy dissipated near the generation sites to the total generated internal tidal energy; it directly modulates the spatial distribution of internal tidal energy (St. Laurent et al., 2002). A lower q value indicates that a larger fraction of internal tidal energy propagates toward the far field as low-mode internal tides. In contrast, a higher q value implies that internal tidal energy is intensively dissipated in the near field, leading to enhanced local mixing (Klymak et al., 2011; Vic et al., 2019). For a long time, to simplify calculations, ocean circulation models have typically prescribed q as a globally uniform constant of 0.3 (Simmons et al., 2004; Saenko and Merryfield, 2005). However, recent studies have demonstrated significant spatial heterogeneity in q. Lefauve et al. (2015) noted its topographic dependence, and Vic et al. (2019) further elucidated that q is regulated by the vertical modal structure of internal tides via a global semi-analytical model. Over small-scale rough topography, high-mode internal tides are predominantly generated, yielding high q values (> 0.8); whereas over large-scale steep topography, low-mode internal tides prevail, leading to low q values (< 0.4). Ignoring the spatiotemporal variability of q causes an order-of-magnitude miscalculation of the mechanical energy supplying internal tidal mixing, thereby significantly reducing the model's capacity to simulate the evolution of water masses and the intensity of global meridional overturning circulation (Cimoli et al., 2019).

As the largest marginal sea in the western Pacific and one of the most well-known hotspots for internal tides, the South China Sea (SCS) is an ideal study area for quantifying internal tidal energy budgets and exploring the spatiotemporal evolution of the dissipation parameter q due to its complex dynamical environment. The SCS not only encompasses the Luzon Strait (LS), a globally recognized strong internal tidal source region (Niwa and Hibiya, 2004; Jan et al., 2007), but also contains complex topographies such as the Nansha Islands (Nansha) and the Dongsha Islands, both located within or adjacent to the basin, which serve as key sink regions for internal tidal energy. Internal tidal energy budget analysis by Wang et al. (2016) revealed that the q in the LS during summer is 0.38, while in the broader SCS it reaches 2.67. Combined with the results of Tian et al. (2025), only a portion of the total internal tides generated in the LS dissipates locally, whereas the majority propagates into the SCS basin in the form of low-mode internal tides and dissipates there. When low-mode internal

https://doi.org/10.5194/egusphere-2026-2713
Preprint. Discussion started: 1 June 2026

tides propagate over rough topography far from the source regions, topographic scattering effects promote the energy transfer to high modes, thereby enhancing local dissipation (Klymak et al., 2010).

Although the generation and propagation of internal tides in the SCS have been extensively explored in previous studies (Zhao et al., 2010; Tian et al., 2025), research on q and its parameterizations remains significantly inadequate. First, existing studies mostly focus on estimating the spatial distribution of q globally and its magnitude in internal tide generation regions. There is a lack of analysis of the temporal variation of q and of systematic comparison of the differences in q between source and sink regions for internal tidal energy. Second, although it is theoretically established that q depends on the internal tidal modal structure and may be related to topographic gradients and the shear intensity of background flow fields (Polzin, 2004; Dunphy and Lamb, 2014), most global ocean circulation models still use empirical constants to set q, neglecting its spatiotemporal variability. Therefore, exploring the spatiotemporal variations of q under different dynamical environments and developing physically consistent parameterizations are essential for accurately simulating internal tidal mixing.

In this study, we intend to diagnose the internal tidal energy budgets, quantify the temporal variations and regional differences of q, and establish parameterizations of q for two representative internal tidal source region (LS) and sink region (Nansha Islands) in the SCS. In Sect. 2, we introduce the utilized data from the MITgcm LLC4320 simulation output, the methods for vertical modal decomposition and internal tidal energy budget analysis, and the eXtreme Gradient Boosting (XGBoost) model employed to predict q. Section 3 presents the results of internal tidal energy budgets and q in the LS and the Nansha Islands, respectively. Specifically, the tidal energy budgets and q are analyzed for each vertical mode separately. Then, the performance of the q parameterizations based on both the physical-based empirical formulation and the XGBoost model is demonstrated. Finally, our results are summarized in Sect. 4.

2 Data and Methods

2.1 Data

The data used in this study are the LLC4320 simulation outputs from the Massachusetts Institute of Technology general circulation model (MITgcm), which solves the Navier-Stokes equations under the hydrostatic and Boussinesq approximations. The model is forced by complete luni-solar tidal potential including 16 principal tidal constituents (such as M_2, S_2, K_1, and O_1) and by the 6-hourly atmospheric reanalysis dataset provided by the European Centre for Medium Range Weather Forecasts (ECMWF) (Marshall et al., 1997; Arbic et al., 2018). An Arakawa-C grid mesh is used in the simulation with a horizontal resolution of 1/48 ° (approximately 2 km in the SCS). In the vertical, the model has 90 z-coordinate levels, with layer thickness increasing from 1 m at the surface to around 480 m near the seabed. The hourly output of three-dimensional velocity, potential temperature, salinity, and sea surface height from September 2011 to November 2012 is used, with specific focus on two key topographic regions, the LS and the Nansha Islands (Fig. 1).

https://doi.org/10.5194/egusphere-2026-2713
Preprint. Discussion started: 1 June 2026

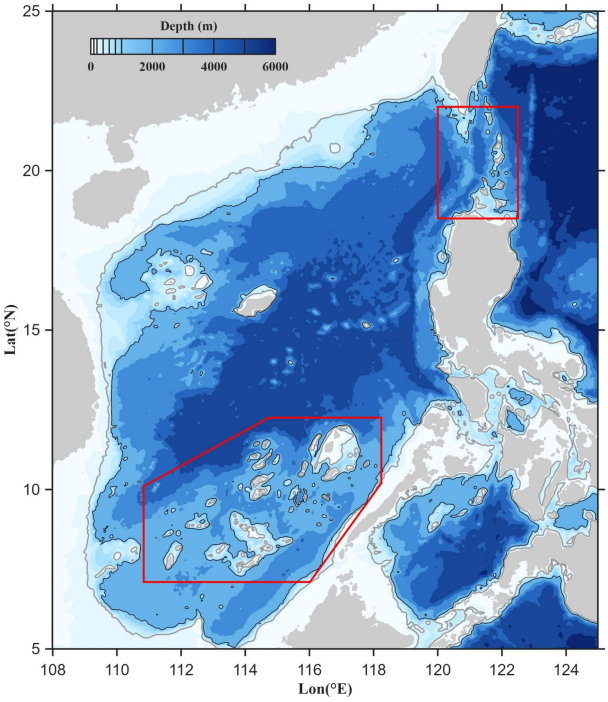

Figure 1. Topography of the SCS. Gray and black contours represent the 200-m and 1000-m isobaths, respectively. Red boxes represent the key topographic regions, including the LS and the Nansha Islands.

2.2 Methods

The subtidal fields ($\overline{\boldsymbol{u}}$ and $\overline{p}$) are obtained by applying a 3-day moving average to the total fields, and the perturbation fields ($\boldsymbol{u}'$,ρ') are obtained by subtracting the subtidal fields from the total ones. The barotropic velocity $\boldsymbol{u}'_{bt}$ is defined as the depth-averaged velocity, and the baroclinic velocity is calculated as $\boldsymbol{u}'_{bc} = \boldsymbol{u}' - \boldsymbol{u}'_{bt}$. A bandpass filter is then applied to extract the diurnal (D1, 0.90–1.10 cpd) and semidiurnal (D2, 1.87–2.10 cpd) tidal constituents. When diagnosing the internal tidal energy budgets and q for individual vertical modes, a vertical modal decomposition method is employed. The modal structure function $\phi_n(z)$ can be obtained by solving the Sturm-Liouville equation (Gill, 1982):

$$\frac{d^2\phi_n(z)}{dz^2} + \frac{N^2(z)}{c_n^2}\phi_n(z) = 0\,, \tag{1}$$

where boundary conditions are given as $\phi_n(0) = \phi_n(-H) = 0$, and H is the water depth. Here, N(z) is the buoyancy frequency, c_n is the eigenspeed, and n is the mode number. Due to the orthogonality of the modes, the baroclinic velocity $\boldsymbol{u}'_{bc}$ and the pressure perturbation p' can be expressed as $\boldsymbol{u}'_{bc}(z,t) = \sum_{n=1}^{N} U_n(t)\varphi_n(z)$, $p'(z,t) = \sum_{n=1}^{N} P_n(t)\varphi_n(z)$, where $\varphi_n(z) = d\phi_n(z)/dz$ is the vertical structure for horizontal velocity and pressure, $U_n(t)$ and $P_n(t)$ are the coefficients of individual modes, and $N = 5$ is the total number of modes used in this study.

https://doi.org/10.5194/egusphere-2026-2713
Preprint. Discussion started: 1 June 2026

To evaluate the generation and dissipation of internal tidal energy, the depth-integrated baroclinic energy equation is used here. After tidal-period averaging and neglecting the tendency and advection terms, the energy equation reduced to (Niwa and Hibiya, 2004):

$$\langle DIS_{bc} \rangle = \langle Conv \rangle - \langle \nabla_h \cdot \boldsymbol{F} \rangle \,, \tag{2}$$

where $\langle \cdot \rangle$ denotes the tidal-period mean. *Conv* is the depth-integrated barotropic-to-baroclinic energy conversion, indicating the local internal tide generation, which can be calculated as:

$$Conv = \int_{-H}^{\eta} \rho' g w'_{bt} \, dz \,, \tag{3}$$

where η is the sea level displacement, and w'_{bt} is the vertical velocity induced by the barotropic tides. This vertical velocity w'_{bt} is given by $w'_{bt} = u'_{bt}\left(\sigma\frac{\partial D}{\partial x} + \frac{\partial \eta}{\partial x}\right) + v'_{bt}\left(\sigma\frac{\partial D}{\partial y} + \frac{\partial \eta}{\partial y}\right) + (\sigma+1)\frac{\partial \eta}{\partial t}$ (Mellor, 2004), where D is the total water depth, $D = H + \eta$, and $\sigma = (z - \eta)/D$. $\boldsymbol{F}$ is the depth-integrated internal tidal energy flux. A positive divergence of $\boldsymbol{F}$ indicates that the internal tidal energy is propagating out of the local area, while a negative value indicates that internal tidal energy is propagating in from the far field. $\boldsymbol{F}$ is given as:

$$\boldsymbol{F} = \int_{-H}^{\eta} \boldsymbol{u}'_{bc} p' dz \,, \tag{4}$$

where p' is calculated as $p'(z,t) = -\frac{1}{H}\int_{-H}^{\eta}\int_{z}^{\eta} g\rho'(\hat{z},t)d\hat{z}dz + \int_{z}^{\eta} g\rho'(\hat{z},t)d\hat{z}$. DIS_{bc} is the depth-integrated local dissipated internal tidal energy. The local internal tidal dissipation efficiency is defined as the ratio of the area-integrated DIS_{bc} to *Conv*, i.e., $q = \int_s ds(DIS_{bc}) \Big/ \int_s ds(Conv)$. Here, the spatial integration domain s corresponds to the red-boxed regions shown in Fig. 1. Based on the above calculations, the internal tidal energy budgets and q for different tidal components and different vertical modes can be estimated. With August and January representing summer and winter respectively, the subsequent analysis is conducted for these two months to present seasonal variation.

To develop a more robust parameterization of q, this study not only adopts a physical-based empirical formulation but also uses the XGBoost model jointly, which can make up for the limitations of traditional physical-based empirical formula in complex dynamic environments. The model inputs include 6 physical features, namely the internal tidal shear averaged within the bottommost 500 m, stratification, barotropic tidal kinetic energy, mode-1 internal tidal energy, the proportion of mode-1 internal tidal energy in the total internal tidal energy, and the mode-1 internal tidal group velocity. The data from the LS and the Nansha Islands are sequentially combined into a training set, a validation set, and a test set with proportions of 70%, 15%, and 15%, respectively. Considering the differences in the physical processes governing q between the internal tidal source regions and sink regions, this study constructs two separate models, one for the LS and one for the Nansha Islands. The Mean Absolute Error (MAE) is adopted as the objective loss function, i.e., $\mathrm{MAE} = \frac{1}{n}\sum_{i=1}^{n} |\hat{y}_i - y_i|$, where y_i and $\hat{y}_i$ denote the true and predicted values, respectively, and n is the number of samples. An early stopping iteration setting of 500 rounds and 800 rounds is applied for both models, respectively.

https://doi.org/10.5194/egusphere-2026-2713
Preprint. Discussion started: 1 June 2026

3 Results

3.1 Local dissipation efficiency of internal tides in the LS

The internal tidal energy budget in the LS is characterized by intense generation, strong outward radiation, and relatively low q. The barotropic-to-baroclinic conversion in the LS ranges from 40 to 50 GW, of which 15–25 GW radiates out of the LS (Fig. 2g), yielding a q value of approximately 0.5 (Fig. 2h). The semidiurnal wavelength better matches the double ridges alignment in the LS, resulting in a larger semidiurnal tide generation (20–30 GW) than diurnal tide generation (10–25 GW) (Fig. 2g). The semidiurnal dissipation (10–20 GW) and q values (0.6–0.8) are also higher than those of the diurnal tide, whose dissipation ranges from 1 to 10 GW and q from 0.1 to 0.6 (Fig. 2g–h). The semidiurnal conversion, dissipation, and q are larger in summer than in winter (Fig. 2g). The diurnal q reaches minima of 0.1 and 0.3 in February–March and June–July, respectively (Fig. 2h).

The summer spatial distributions demonstrate that internal tide generation and dissipation are concentrated over and around the double ridges (Fig. 2a–b and 2e–f). Substantial internal tidal energy propagates westward and northwestward from the western ridge into the SCS (Fig. 2c–d). The semidiurnal component plays a dominant role in the internal tide generation and dissipation (Fig. 2a–b, 2e–g). The q values ranging from 0.49 to 0.57 in the LS are comparable to those in other representative internal tide generation regions; for example, You et al. (2023) estimated a q value of about 0.58 for the M_2 internal tide at the Aleutian Ridge, suggesting that q values in submarine ridges serving as internal tide source regions share a similar magnitude.

The internal tidal energy budgets and q in the LS exhibit differences among individual tidal components and vertical modes. Both diurnal and semidiurnal internal tide generation are dominated by modes 1–2, with mode 1 accounting for roughly 50% of the total generation and exhibiting an energy flux divergence greater than those of other modes (Fig. 3j–k). The divergence of diurnal mode-1 energy flux is even larger in magnitude than the local generation (Fig. 3j), resulting in negative q values (Fig. 3*l*), implying that the internal tidal energy generated in the LS radiates outward as low-mode internal tides intensively. Tian et al. (2025) indicated that the diurnal tide has a larger decay scale than the semidiurnal tide, which favors more outward radiation of the diurnal tide as mode 1. By contrast, although the semidiurnal energy budget is also dominated by modes 1–2, the proportion of mode-1 energy flux divergence is relatively smaller, and its seasonal variability is weaker than that of the diurnal tide (Fig. 3j–k). Regarding local dissipation, q for modes 3–5 of both the diurnal and semidiurnal components ranges from 0.8 to 2.7, significantly larger than that of modes 1–2 (< 0.8) (Fig. 3*l*–m).

The strongly positive generation regions for modes 1–2 internal tides are concentrated at the crests of the double ridges, whereas the high-generation regions for mode 3 are distributed along the ridge flanks (Fig. 3a–c). The energy budget of the mode-1 internal tide is characterized by substantial energy propagating northwestward and westward into the SCS, as well as eastward into the Pacific Ocean (Fig. 3d). The majority of the mode-1 semidiurnal energy flux enters the SCS, with peak values reaching 25 kW m^{-1} (Fig. 3d). Local dissipation gradually weakens and becomes spatially dispersed with increasing mode number (Fig. 3d–f). At the Mid-Atlantic Ridge and the Hawaiian Ridge, Vic et al. (2018) indicated that a dominant

https://doi.org/10.5194/egusphere-2026-2713
Preprint. Discussion started: 1 June 2026

proportion of mode-1 internal tide generation facilitates the outward radiation of substantial energy as low-mode internal tides, yielding small q values. This result confirms the robust far-field radiation capacity of internal tides and the smaller q values of mode 1 relative to those of higher modes in the LS.

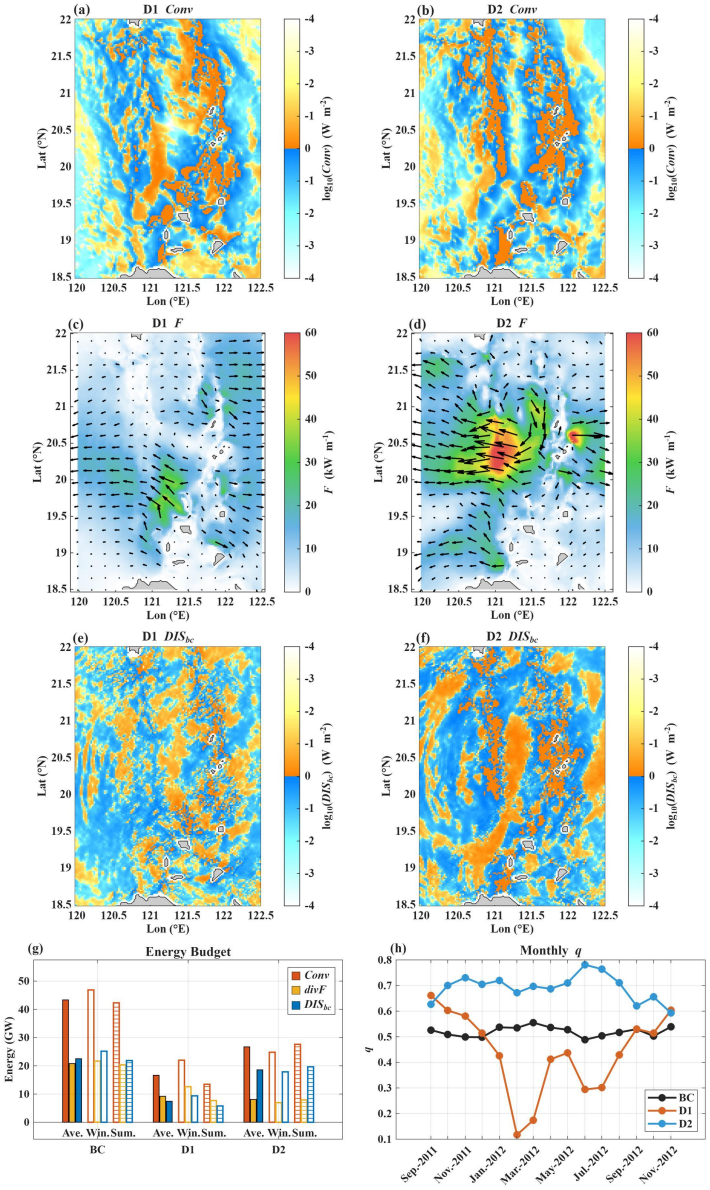

Figure 2. (a–f) Spatial distributions of the internal tidal energy budget terms in the LS during summer, (g) bar chart of these budget terms, and (h) time series of the monthly mean local internal tidal dissipation efficiency, q. BC, D1, and D2 represent the total internal tide, diurnal tide, and semidiurnal tide, respectively. "Ave.", "Win.", and "Sum." stand for the annual-, winter-, and summer-mean values, respectively. $\langle Conv \rangle$ is the tidal-period mean depth-integrated barotropic-to-baroclinic energy conversion, $\langle F \rangle$ is the tidal-period mean depth-integrated internal tidal energy flux, $\langle divF \rangle$ is the tidal-period mean divergence of the depth-integrated internal tidal energy flux, and $\langle DIS_{bc} \rangle$ is the tidal-period mean depth-integrated local internal tidal dissipation. In (a–b) and (e–f), the units for *Conv* and DIS_{bc} are W m^{-2}, with orange (blue) representing positive (negative) values. In (c–d), the unit for F is kW m^{-1}, with colors representing magnitude and arrows indicating vectors. In (g), the units for *Conv*, *divF*, and DIS_{bc} are GW.

https://doi.org/10.5194/egusphere-2026-2713
Preprint. Discussion started: 1 June 2026

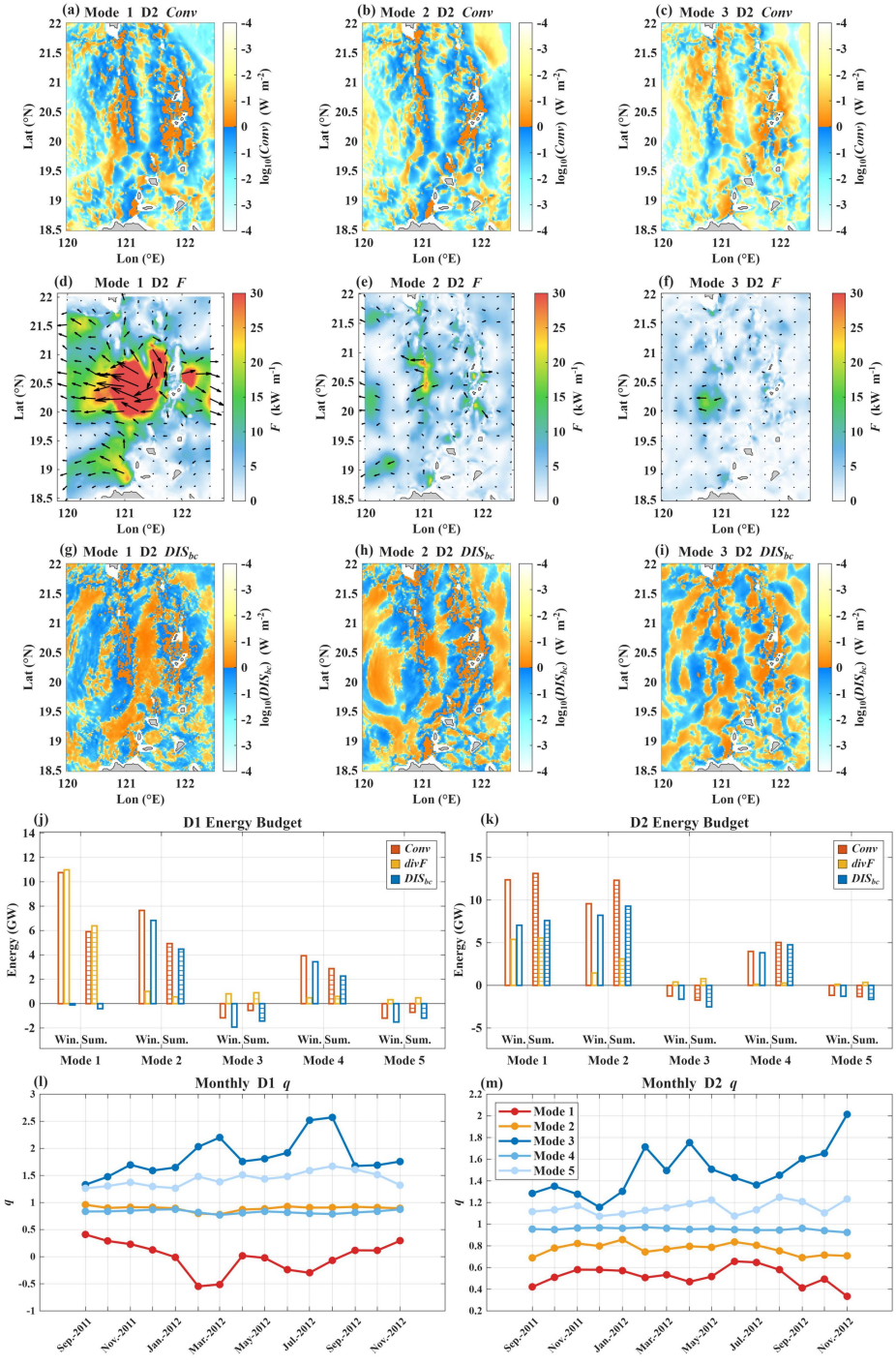

185 **Figure 3. (a–i) Spatial distributions of the semidiurnal internal tidal energy budget terms for modes 1–3 in the LS during summer, (j–k) bar charts of the energy budget terms for modes 1–5, and (l–m) time series of the monthly mean *q* for modes 1–5. D1 and D2 represent the diurnal and semidiurnal tides, respectively. "Win." and "Sum." represent winter and summer, respectively. In (a–c) and (g–i), the units for *Conv* and DIS_{bc} are W m^{-2}, with orange (blue) indicating positive (negative) values. In (d–f), the unit for *F* is kW m^{-1}, with colors indicating magnitude and arrows indicating vectors. In (j–k), the units for *Conv*, *divF*, and DIS_{bc} are GW.**

https://doi.org/10.5194/egusphere-2026-2713
Preprint. Discussion started: 1 June 2026

3.2 Local dissipation efficiency of internal tides in the Nansha Islands

In contrast to the LS, the internal tidal energy budget of the Nansha Islands is characterized by low local generation, strong energy convergence, and a high value of q. The local generation of internal tides in the Nansha Islands is weak, fluctuating between 0.6 and 1.3 GW, whereas the incoming internal tidal energy flux can reach 1.5 GW (Fig. 4g). This energy budget (dominated by far-field input) directly elevates q values to 1–3 (Fig. 4h). Both the local generation and the energy flux of the diurnal tide dominate those of the semidiurnal tide (Fig. 4g), maintaining the q of diurnal tide in the range of 1.5–2, which is larger than the q of semidiurnal tide varying between 1.0 and 1.5 (Fig. 4h).

Both the generation and local dissipation of internal tides in the Nansha Islands exhibit a scattered patchy pattern, with high values concentrated around reefs (Fig. 4a–b and 4e–f). All the energy budget terms of the diurnal tide are larger than those of the semidiurnal tide (Fig. 4a–f), with a significant incoming diurnal energy flux of approximately 1.5 kW m^{-1} at the southwestern and northern boundaries of the Nansha Islands (Fig. 4c). Lahaye et al. (2020) demonstrated that incident low-mode internal tides can be scattered to higher modes through interactions with steep topography. Subsequently, high-mode internal tides are susceptible to breaking in their generation regions (Siyanbola et al., 2024). It is therefore reasonable that far-field internal tidal beams trigger intense topographic scattering, which supply sufficient energy to sustain high local dissipation efficiency ($q > 1$) despite weak local generation in this region.

In terms of vertical modes, the internal tidal energy budget terms in the Nansha Islands are significantly smaller in magnitude than those in the LS, with strong low-mode energy convergence and high values of q. The energy budget in the Nansha Islands is dominated by modes 1 and 2 (Fig. 5j–k). Unlike in the LS, here the local generation of mode 1 is weaker than that of mode 2 (Fig. 5j–k). This energy budget, dominated by far-field input of mode-1 energy flux, directly results in the q values of mode 1 ($q > 2$) exceeding those of mode 2 ($q < 2$), as shown in Fig. 5*l*–m. The energy budget terms for modes 3–5 are all near zero with highly variable q (Fig. 5j–m), indicating that locally generated high modes are not the primary contributors to dissipation. Diurnal tides dominate in the Nansha Islands, with all energy budget terms exceeding those of the semidiurnal tide and showing pronounced seasonal variability (Fig. 5j–k). The q values of the mode-1 diurnal tide can reach a maximum of 5 (Fig. 5*l*).

In the Nansha Islands, all internal tidal energy budget terms decrease with increasing mode number, except for the mode-2 energy conversion (Fig. 5a–i). The mode-3 energy budget terms are generally less than one-third of those for modes 1–2. Two dominant incoming energy fluxes exist in the Nansha Islands, originating from the northeast and the southwest, respectively. With increasing mode number, the energy flux from the southwestern shelf slope of the SCS decays more rapidly than that from the northeastern source, suggesting that the reflection from the southwestern shelf slope of the SCS may furnish local dissipation in the Nansha Islands. Siyanbola et al. (2024) pointed out that in weak generation regions, intense local dissipation depends on the sufficient convergence and slope reflection of far-field low-mode internal tidal beams. This is consistent with our results that the elevated mode-1 dissipation and q (> 2) in the Nansha Islands are

https://doi.org/10.5194/egusphere-2026-2713
Preprint. Discussion started: 1 June 2026

potentially dominated by the incoming mode-1 energy flux, particularly the reflection from the southwestern shelf slope of the SCS.

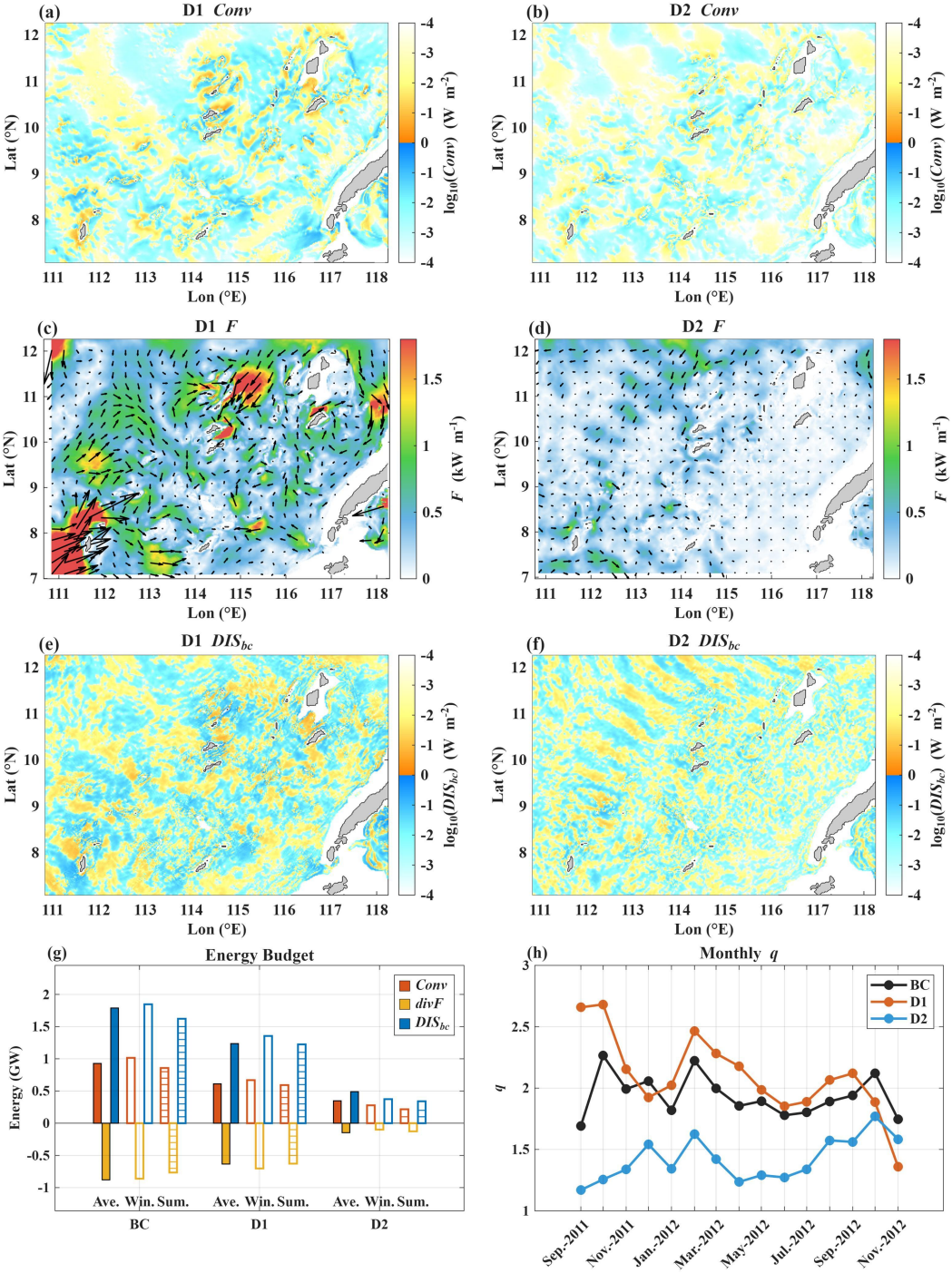

225 **Figure 4. Same as Fig. 2, but for the Nansha Islands.**

https://doi.org/10.5194/egusphere-2026-2713
Preprint. Discussion started: 1 June 2026

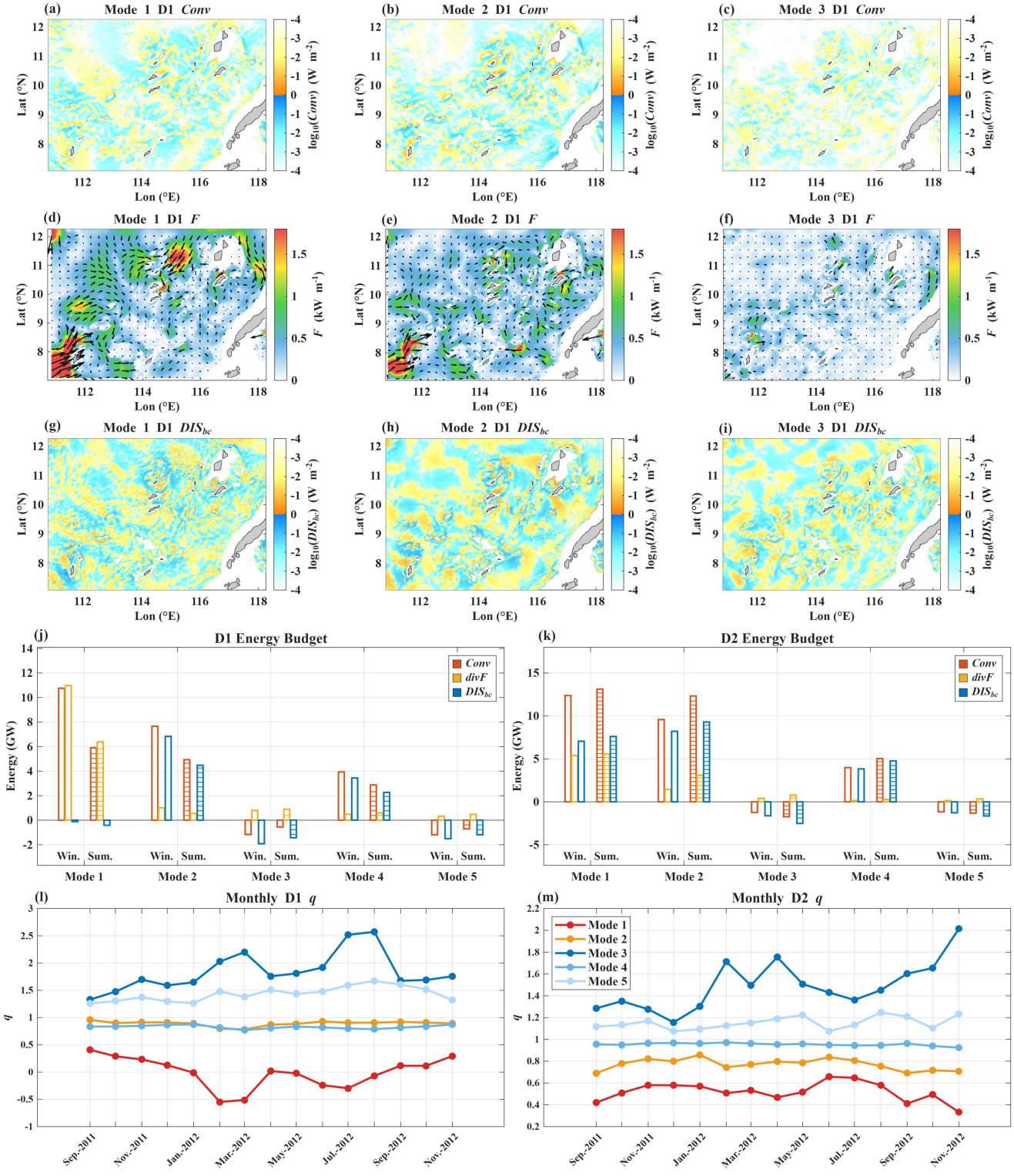

Figure 5. Same as Fig. 3, but for the Nansha Islands and (a–i) for diurnal internal tide.

https://doi.org/10.5194/egusphere-2026-2713
Preprint. Discussion started: 1 June 2026

3.3 Parameterizations for the local dissipation efficiency of internal tides

3.3.1 Parameterization constrained by physical factors

To develop parameterizations for q that are applicable to dynamically distinct regions, 3 key physical parameters are chosen based on the features of diurnal and semidiurnal tides in the LS and the Nansha Islands. The depth-averaged internal tidal shear (S^2) within the bottommost 500 m represents the local internal wave intensity; the barotropic tidal kinetic energy (E_{BT}) quantifies the local tidal forcing strength; and the mode-1 internal tidal energy ($E^{(1)}$) is used to represent the potential for radiating low-mode energy to the far field. A dimensionless power-law function is fitted to the 429-day time series of q via multiple regression, with the specific formula expressed as

$$q_{para} = q_0\left(\frac{S^2}{S_0^2}\right)^{a_1}\left(\frac{E_{BT}}{E_{BT0}}\right)^{a_2}\left(\frac{E^{(1)}}{E_0^{(1)}}\right)^{a_3} + q_b\,, \tag{5}$$

where S_0^2, E_{BT0} and $E_0^{(1)}$ are the time-mean reference values of each variable within each region; q_0 is the amplitude coefficient, q_{b} is a constant representing the background state; and a_1, a_2 and a_3 are the power-law exponents corresponding to the internal tidal shear, barotropic tidal kinetic energy, and mode-1 internal tidal energy, respectively.

Table 1 presents the fitting coefficients and associated errors for this physical parameterization of q for diurnal and semidiurnal tides in both the LS and the Nansha Islands. In the LS, the coefficients of determination (R^2) for the diurnal and semidiurnal tides are both 0.35, with root mean square error (RMSE) of 0.14 and 0.08, respectively. The fitted parameters characterize the dynamical process modulating q in the LS. For both diurnal and semidiurnal components, a_2 representing the sensitivity to barotropic tidal kinetic energy is positive (0.40 and 0.37, respectively), whereas a_3 representing the sensitivity to mode-1 internal tidal energy is negative (-0.31 and -0.40, respectively). Stronger local barotropic forcing therefore enhances internal tide generation and local dissipation, leading to a positive modulation of q. Conversely, when mode-1 internal tide energy accumulates substantially, the internal tide tends to propagate to the far field as coherent beams, thereby reducing q relatively. The background state constant q_{b} in the LS (0.05 and 0.15, respectively) is smaller than the amplitude coefficient q_0 (0.44 and 0.55, respectively). As shown in Fig. 6, the parameterization captures the mean state of q in the LS, although it exhibits some smoothing toward extreme values, manifesting as overestimation at low q and underestimation at high q.

The parameterized q in the Nansha Islands reveals a dynamical process different from that of the LS. As shown in Table 1, the R^2 values for diurnal and semidiurnal tides are 0.26 and 0.48, respectively. For both diurnal and semidiurnal components, a_2 for barotropic tidal kinetic energy is negative (-0.98 and -2.13, respectively), whereas a_3 for mode-1 energy is positive (0.91 and 2.05, respectively). This indicates that when weakened local barotropic forcing reduces internal tide generation, q tends to increase, provided that the far-field low-mode energy remains elevated and drives intense local dissipation. In contrast to the LS, the background constants q_{b} for diurnal and semidiurnal tides in the Nansha Islands (1.47 and 1.06, respectively) substantially exceed the corresponding amplitude coefficients q_0 (0.69 and 0.38, respectively). This

https://doi.org/10.5194/egusphere-2026-2713
Preprint. Discussion started: 1 June 2026

suggests that topographic scattering and reflection by the widespread seamounts and reefs, together with the incoming low-mode internal tidal energy, sustain q at a high level above 1.

Table 1. Fitting coefficients and associated errors of the physical parameterization for q in the LS and the Nansha Islands.

Region-Band	q_0	q_b	a_1	a_2	a_3	R^2	RMSE
LS-D1	0.44	0.05	-0.27	0.40	-0.31	0.35	0.14
LS-D2	0.55	0.15	-0.02	0.37	-0.40	0.35	0.08
Nansha-D1	0.69	1.47	0.57	-0.98	0.91	0.26	0.67
Nansha-D2	0.39	1.06	-0.48	-2.13	2.05	0.48	0.48

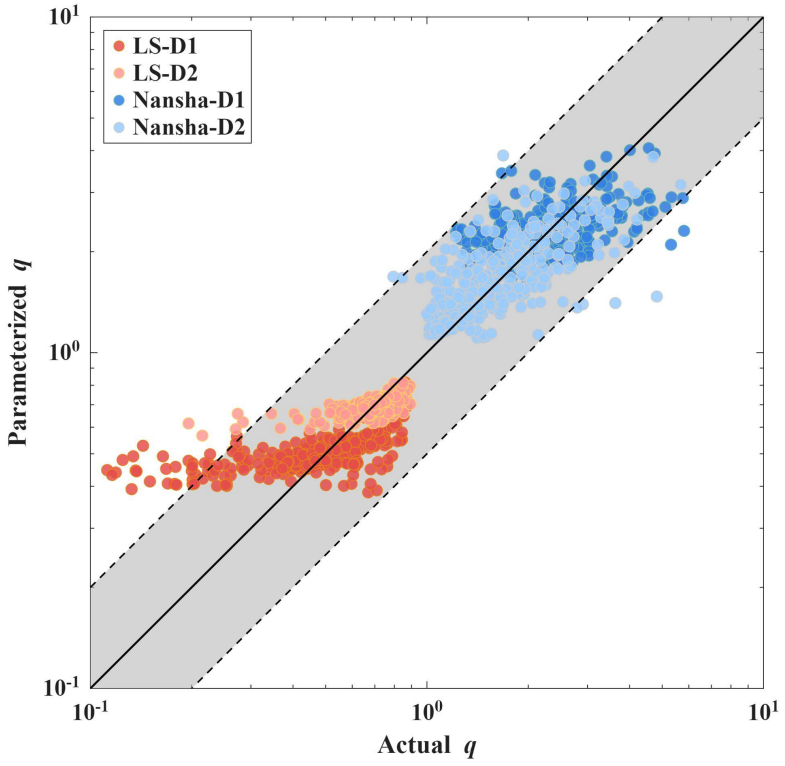

Figure 6. Scatter plot of parameterized q versus actual q for the LS and the Nansha Islands. The black line denotes the 1:1 reference line, and the two outer black dashed lines represent the 2:1 and 1:2 bounds.

3.3.2 Parameterization based on the XGBoost model

The XGBoost model achieves solid predictive performance on the combined testing set spanning both regions and tidal components, with an R^2 of 0.65 and an RMSE of 0.38 (Table 2). When predicting the semidiurnal component independently, the R^2 reaches 0.52. As shown in Fig. 7, the great overall performance of the model primarily stems from its ability to

https://doi.org/10.5194/egusphere-2026-2713
Preprint. Discussion started: 1 June 2026

achieve clear macroscopic clustering across regions, separating the data into a low-q cluster for the LS and a high-q cluster for the Nansha Islands.

However, the predictive performance of the XGBoost model degrades markedly when predicting individual regions and tidal components separately. Table 2 shows that the R^2 values for diurnal and semidiurnal tides in the LS decrease to 0.39 and 0.11, respectively. The R^2 for the semidiurnal tide in the Nansha Islands is 0.30, and that for the diurnal tide is negative. As shown in Fig. 7, the model predictions for the LS are relatively concentrated and clustered along the 1:1 reference line, whereas those for the Nansha Islands exhibit greater dispersion. This degradation likely arises from the fact that extreme q values are highly sensitive to the topographic scattering of far-field low-mode internal tides and nonlinear wave-wave interactions.

As noted by Zhao et al. (2010), long-range internal tides form spatially complex interference patterns through superposition from multiple sources, with phase differences further modulated by mesoscale refraction. These far-field inputs and mesoscale processes are not captured by the local area-averaged input features employed here, which inevitably smooth out interference signals. Consequently, the XGBoost model broadly captures the phase of q variability over the spring-neap tidal cycles and predicts the temporal evolution of q well (Fig. 8), although its predictions of q exhibit a degree of smoothing.

Table 2. Performance of the XGBoost model on the testing set.

Region	Band	RMSE	R^2
LS, Nansha	D1, D2	0.38	0.65
LS, Nansha	D1	0.36	0.75
LS, Nansha	D2	0.40	0.52
LS	D1	0.14	0.39
LS	D2	0.08	0.11
Nansha	D1	0.50	-1.69
Nansha	D2	0.57	0.30

https://doi.org/10.5194/egusphere-2026-2713
Preprint. Discussion started: 1 June 2026

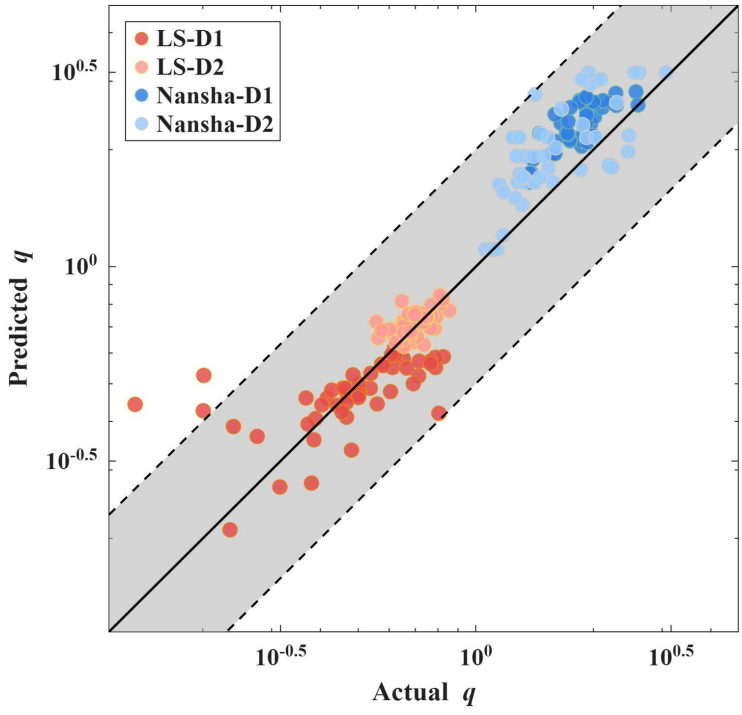

Figure 7. Scatter plot of the predicted *q* from the XGBoost model versus the actual *q* for the LS and the Nansha Islands. The black line represents the 1:1 reference line, and the two outer black dashed lines represent the 2:1 and 1:2 bounds.

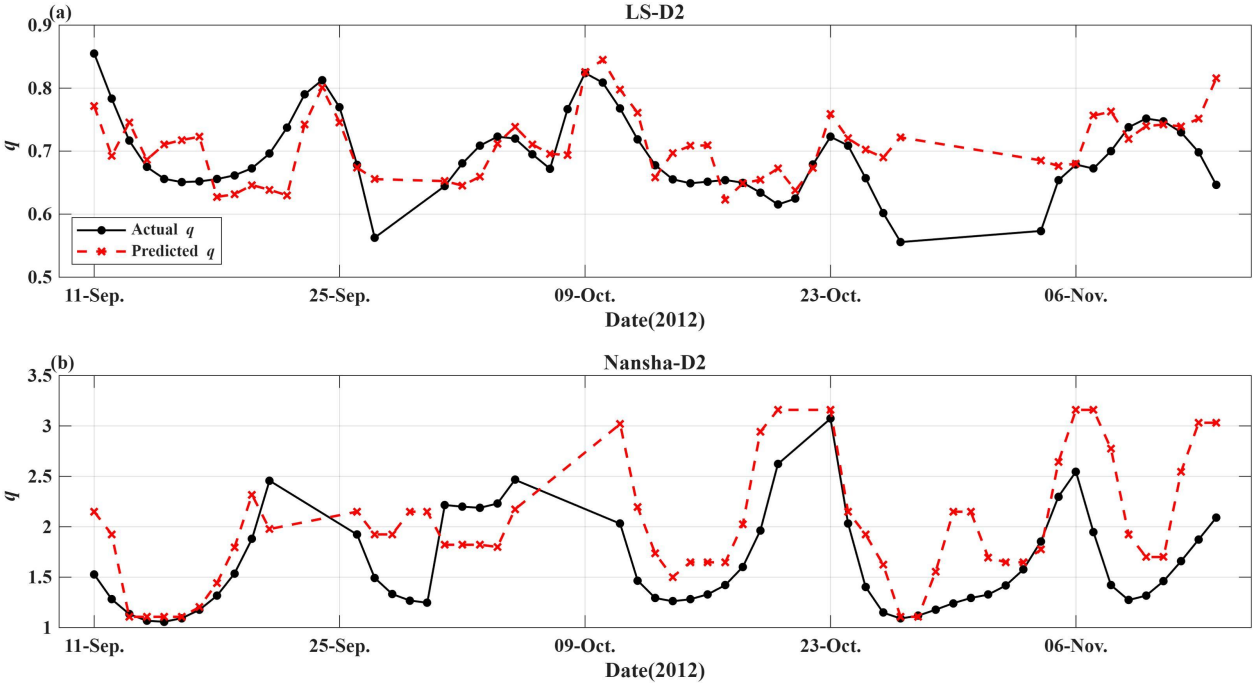

Figure 8. Time series of the predicted *q* from the XGBoost model and the actual *q* for the semidiurnal tide in (a) the LS and (b) the Nansha Islands.

https://doi.org/10.5194/egusphere-2026-2713
Preprint. Discussion started: 1 June 2026

4 Summary

Based on the LLC4320 simulation, we reveal differences in the local internal tidal dissipation efficiency (q) between the source region (represented by the LS) and the sink region (represented by the Nansha Islands). In the LS, the value of q ranges from 0.3 to 0.7, which is consistent with earlier results. The mode-1 energy flux radiates intensively out of the LS, resulting in q values smaller than those of other higher modes. This confirms that in generation regions of internal tides, much of the baroclinic energy propagates to the far field as low modes rather than dissipating locally. Conversely, in the Nansha Islands, q is generally larger than 1, especially the q values of the mode-1 diurnal and semidiurnal tides are consistently larger than those of higher modes. The reason for $q > 1$ is that the far-field internal tidal energy flux entering the Nansha Islands exceeds the locally generated one. Thus, the primary source for local dissipation is not the locally generated internal tide, but rather far-field internal tidal beams propagating from the LS.

The physical-based empirical formulation and the XGBoost model used to scale q in this study successfully capture the macroscopic clustering of the mean states of q in both the LS and the Nansha Islands. They also reproduce the periodic temporal variation of q, with an R^2 value reaching 0.65. Moreover, the physical parameterization results reveal regional differences in the dominant mechanisms modulating q. In the LS, while intense barotropic forcing generates energetic internal tides and enhances local dissipation, the substantial accumulation of mode-1 internal tidal energy favors the radiation of coherent beams into the far field, thereby reducing q. In the Nansha Islands, the negative power-law coefficient (a_2) for barotropic tidal kinetic energy, along with the positive coefficient (a_3) for mode-1 internal tidal energy, indicates that local dissipation is dominated by far-field energy input. Furthermore, the scattering and reflection of internal tides by the widespread seamounts and reefs play a dominant role in sustaining high q in the Nansha Islands. On the other hand, the XGBoost model yields a consistent periodic temporal change and accurately predicts the mean q value in both source and sink regions, despite with some quantitative discrepancies. However, those far-field inputs and mesoscale processes are not captured by the local area-averaged input features, resulting in a degree of smoothing in the predicted q. This insight suggests that future parameterizations of q and internal tide mixing must move beyond the traditional framework that relies solely on local generation; instead, they should explicitly and thoughtfully incorporate the nonlocal processes, e.g., the far-field propagation of internal wave field experiencing interference and scattering.

Data availability

The MITgcm LLC4320 data that support the findings of this study are openly available at https://data.nas.nasa.gov/ecco/data.php?dir=/eccodata/llc_4320.

https://doi.org/10.5194/egusphere-2026-2713
Preprint. Discussion started: 1 June 2026

Author contributions

The study was conceived and designed by QY. Data preparation, material collection, and analysis were performed by ZY and HS. ZY and HS prepared the manuscript with contributions from all co-authors.

Competing interests

The contact author has declared that none of the authors has any competing interests.

Disclaimer

Publisher's note: Copernicus Publications remains neutral with regard to jurisdictional claims made in the text, published maps, institutional affiliations, or any other geographical representation in this paper. While Copernicus Publications makes every effort to include appropriate place names, the final responsibility lies with the authors. Views expressed in the text are those of the authors and do not necessarily reflect the views of the publisher.

Acknowledgements

Financial support

This work was supported by National Natural Science Foundation of China (Grants 42376012, 42506011, 42076012 and 42006012).

References

Arbic, B. K., Alford, M., Ansong, J., Buijsman, M., Ciotti, R., Farrar, J., Hallberg, R., Henze, C., Hill, C., Luecke, C., Menemenlis, D., Metzger, E., Müeller, M., Nelson, A., Nelson, B., Ngodock, H., Ponte, R., Richman, J., Savage, A., and Zhao, Z.: A primer on global internal tide and internal gravity wave continuum modeling in HYCOM and MITgcm, in New Frontiers in Operational Oceanography, edited by: Chassignet, E. P., Pascual, A., Tintoré, J., and Verron, J., GODAE Ocean View, 307–392, https://doi.org/10.17125/gov2018.ch13, 2018.

Cimoli, L., Caulfield, C. P., Johnson, H. L., Marshall, D. P., Mashayek, A., Naveira Garabato, A. C., and Vic, C.: Sensitivity of deep ocean mixing to local internal tide breaking and mixing efficiency, Geophys. Res. Lett., 46, 14622 – 14633, https://doi.org/10.1029/2019GL085056, 2019.

https://doi.org/10.5194/egusphere-2026-2713
Preprint. Discussion started: 1 June 2026

de Lavergne, C., Vic, C., Madec, G., Roquet, F., Waterhouse, A. F., Whalen, C. B., Cuypers, Y., Bouruet-Aubertot, P., Ferron, B. and Hibiya, T.: A parameterization of local and remote tidal mixing, J. Adv. Model. Earth Sy., 12, e2020MS002065, https://doi.org/10.1029/2020MS002065, 2020.

Dunphy, M. and Lamb, K. G.: Focusing and vertical mode scattering of the first mode internal tide by mesoscale eddy interaction, J. Geophys. Res.-Oceans, 119, 523–536, https://doi.org/10.1002/2013JC009293, 2014.

Egbert, G. D. and Ray, R. D.: Significant dissipation of tidal energy in the deep ocean inferred from satellite altimeter data, Nature, 405, 775–778, https://doi.org/10.1038/35015531, 2000.

Egbert, G. D. and Ray, R. D.: Semi-diurnal and diurnal tidal dissipation from TOPEX/Poseidon altimetry, Geophys. Res. Lett., 30, 1907, https://doi.org/10.1029/2003GL017676, 2003.

Ferrari, R. and Wunsch, C.: Ocean circulation kinetic energy: Reservoirs, sources, and sinks, Annu. Rev. Fluid Mech., 41, 253–282, https://doi.org/10.1146/annurev.fluid.40.111406.102139, 2009.

Garrett, C. and Kunze, E.: Internal tide generation in the deep ocean, Annu. Rev. Fluid Mech., 39, 57–87, https://doi.org/10.1146/annurev.fluid.39.050905.110227, 2007.

Gill, A.: Atmosphere-ocean dynamics, in: 1st Edn., Academic Press, New York, 680 pp., ISBN 978-0-12-283522-3, 1982.

Jan, S., Chern, C., Wang, J., and Chao, S.: Generation of diurnal K_1 internal tide in the Luzon Strait and its influence on surface tide in the South China Sea, J. Geophys. Res., 112, C06019, https://doi.org/10.1029/2006JC004003, 2007.

Jayne, S. R.: The impact of abyssal mixing parameterizations in an ocean general circulation model, J. Phys. Oceanogr., 39, 1756–1775, https://doi.org/10.1175/2009JPO4085.1, 2009.

Klymak, J. M., Alford, M. H., Pinkel, R., Lien, R., Yang, Y. J., and Tang, T.: The breaking and scattering of the internal tide on a continental slope, J. Phys. Oceanogr., 41, 926–945, https://doi.org/10.1175/2010JPO4500.1, 2011.

Klymak, J. M., Legg, S., and Pinkel, R.: A simple parameterization of turbulent tidal mixing near supercritical topography, J. Phys. Oceanogr., 40, 2059–2074, https://doi.org/10.1175/2010JPO4396.1, 2010.

Lahaye, N., Gula, J., and Roullet, G.: Internal tide cycle and topographic scattering over the North Mid-Atlantic Ridge, J. Geophys. Res.-Oceans, 125, e2020JC016376, https://doi.org/10.1029/2020JC016376, 2020.

Lefauve, A., Muller, C., and Melet, A.: A three-dimensional map of tidal dissipation over abyssal hills, J. Geophys. Res.-Oceans, 120, 4760–4777, https://doi.org/10.1002/2014JC010598, 2015.

MacKinnon, J. A., Zhao, Z., Whalen, C. B., Waterhouse, A. F., Trossman, D. S., Sun, O. M., Laurent, L. C. S., Simmons, H. L., Polzin, K., Pinkel, R., Pickering, A., Norton, N. J., Nash, J. D., Musgrave, R., Merchant, L. M., Melet, A. V., Mater, B., Legg, S., Large, W. G., Kunze, E., Klymak, J. M., Jochum, M., Jayne, S. R., Hallberg, R. W., Griffies, S. M., Diggs, S., Danabasoglu, G., Chassignet, E. P., Buijsman, M. C., Bryan, F. O., Briegleb, B. P., Barna, A., Arbic, B. K., Ansong, J. K., and Alford, M. H.: Climate process team on internal wave-driven ocean mixing, Bull. Amer. Meteorol. Soc., 98, 2429–2454, https://doi.org/10.1175/BAMS-D-16-0030.1, 2017.

Marshall, J., Adcroft, A., Hill, C., Perelman, L., and Heisey, C.: A finite-volume, incompressible Navier Stokes model for studies of the ocean on parallel computers, J. Geophys. Res., 102(C3), 5753–5766, https://doi.org/10.1029/96JC02775, 1997.

https://doi.org/10.5194/egusphere-2026-2713
Preprint. Discussion started: 1 June 2026

Melet, A., Legg, S., and Hallberg, R.: Climatic impacts of parameterized local and remote tidal mixing, J. Climate, 29, 3473–3500, https://doi.org/10.1175/JCLI-D-15-0153.1, 2016.

Mellor, G. L.: Users guide for a three-dimensional primitive equation numerical ocean model, Princeton Univ., Princeton, NJ, 08544–10710, 2004.

Munk, W. H. and Wunsch, C.: Abyssal recipes II: Energetics of tidal and wind mixing, Deep-Sea Res., 45, 1977–2010, https://doi.org/10.1016/S0967-0637(98)00070-3, 1998.

Niwa, Y. and Hibiya, T.: Three-dimensional numerical simulation of M_2 internal tides in the East China Sea, J. Geophys. Res., 109, 2003JC001923, https://doi.org/10.1029/2003JC001923, 2004.

Nycander, J.: Generation of internal waves in the deep ocean by tides, J. Geophys. Res., 110, C10028, https://doi.org/10.1029/2004JC002487, 2005.

Polzin, K.: A heuristic description of internal wave dynamics, J. Phys. Oceanogr., 34, 214–230, https://doi.org/10.1175/1520-0485(2004)034<0214:AHDOIW>2.0.CO;2, 2004.

Saenko, O. A. and Merryfield, W. J.: On the effect of topographically enhanced mixing on the global ocean circulation, J. Phys. Oceanogr., 35, 826–834, https://doi.org/10.1175/JPO2722.1, 2005.

Simmons, H. L., Jayne, S. R., St. Laurent, L. C., and Weaver, A. J.: Tidally driven mixing in a numerical model of the ocean general circulation, Ocean Modell., 6, 245–263, https://doi.org/10.1016/S1463-5003(03)00011-8, 2004.

Siyanbola, O. Q., Buijsman, M. C., Delpech, A., Barkan, R., Pan, Y., and Arbic, B. K.: Interactions of remotely generated internal tides with the U.S. West Coast continental margin, J. Geophys. Res.-Oceans, 129, e2023JC020859, https://doi.org/10.1029/2023JC020859, 2024.

St. Laurent, L. C., Simmons, H. L., and Jayne, S. R.: Estimating tidally driven mixing in the deep ocean, Geophys. Res. Lett., 29, 2106, https://doi.org/10.1029/2002GL015633, 2002.

St. Laurent, L. C. and Garrett, C.: The role of internal tides in mixing the deep ocean, J. Phys. Oceanogr., 32, 2882–2899, https://doi.org/10.1175/1520-0485(2002)032<2882:TROITI>2.0.CO;2, 2002.

Tian, Y., Bai, X., Wang, C., and Liu, Z.: Tidal energetics in the eddying South China Sea from a high-resolution numerical simulation, Prog. Oceanogr., 231, 103418, https://doi.org/10.1016/j.pocean.2025.103418, 2025.

Vic, C., Naveira Garabato, A. C., Green, J. A. M., Spingys, C., Forryan, A., Zhao, Z., and Sharples, J.: The lifecycle of semidiurnal internal tides over the Northern Mid-Atlantic Ridge, J. Phys. Oceanogr., 48, 61–80, https://doi.org/10.1175/JPO-D-17-0121.1, 2018.

Vic, C., Naveira Garabato, A. C., Green, J. M., Waterhouse, A. F., Zhao, Z., Melet, A., de Lavergne, C., Buijsman, M. C., and Stephenson, G. R.: Deep-ocean mixing driven by small-scale internal tides, Nat. Commun., 10, 2099, https://doi.org/10.1038/s41467-019-10149-5, 2019.

Wang, X., Peng, S., Liu, Z., Huang, R. X., Qian, Y., and Li, Y.: Tidal mixing in the South China Sea: An estimate based on the internal tide energetics, J. Phys. Oceanogr., 46, 107–124, https://doi.org/10.1175/JPO-D-15-0082.1, 2016.

https://doi.org/10.5194/egusphere-2026-2713
Preprint. Discussion started: 1 June 2026

Waterhouse, A. F., MacKinnon, J. A., Nash, J. D., Alford, M. H., Kunze, E., Simmons, H. L., Polzin, K. L., Laurent, L. C. S., Sun, O. M., Pinkel, R., Talley, L. D., Whalen, C. B., Huussen, T. N., Carter, G. S., Fer, I., Waterman, S., Naveira Garabato, A. C., Sanford, T. B., and Lee, C. M.: Global patterns of diapycnal mixing from measurements of the turbulent dissipation rate, J. Phys. Oceanogr., 44, 1854–1872, https://doi.org/10.1175/JPO-D-13-0104.1, 2014.

Wunsch, C. and Ferrari, R.: Vertical mixing, energy, and the general circulation of the oceans, Annu. Rev. Fluid Mech., 36, 281–314, https://doi.org/10.1146/annurev.fluid.36.050802.122121, 2004.

You, J., Xu, Z., Li, Q., Zhang, P., Yin, B., and Hou, Y.: M_2 Internal tide energetics and behaviors in the Subpolar North Pacific, J. Phys. Oceanogr., 53, 1269–1290, https://doi.org/10.1175/JPO-D-22-0032.1, 2023.

Zhao, Z., Alford, M. H., MacKinnon, J. A., and Pinkel, R.: Long-range propagation of the semidiurnal internal tide from the Hawaiian Ridge, J. Phys. Oceanogr., 40, 713–736, https://doi.org/10.1175/2009JPO4207.1, 2010.